First-principles studies of liquid lithium under pressure

2010 J. Phys.: Condens. Matter 22 095503

(http://iopscience.iop.org/0953-8984/22/9/095503)

J. Phys.: Condens. Matter **22** (2010) 095503 (7pp) doi:10.1088/0953-8984/22/9/095503

First-principles studies of liquid lithium under pressure

Jianjun Yang[1], John S Tse[1,2,3] and Toshiaki Iitaka[2]

[1] Department of Physics and Engineering Physics, University of Saskatchewan, Saskatoon, SK, S7N 5E2, Canada
[2] Computational Astrophysics Laboratory, RIKEN, 2-1 Hirosawa, Wako, Saitama, 351-0198, Japan

E-mail: John.Tse@usask.ca

Received 5 October 2009, in final form 14 January 2010
Published 10 February 2010
Online at stacks.iop.org/JPhysCM/22/095503

Abstract
Effects of compression on the structural and electronic properties of liquid lithium are investigated with first-principles molecular dynamics calculations. Within a large pressure range up to 60 GPa, along isotherms from 600 to 1000 K, several structural transformations were found. The liquid structures at high pressure are found to be not sensitive to the temperature within this range. It is shown that the radial distribution functions broadly resemble the corresponding solid phases, particularly at low pressures. The evolution of the electronic structure under pressure also shows a remarkable similarity to the underlying solid. However, detailed analyses of the temporal liquid inherent structures show that the instantaneous short-range order may differ significantly from the underlying known solid phase.

(Some figures in this article are in colour only in the electronic version)

1. Introduction

Recent studies of liquid Na [1] and Cs [2] under pressure revealed the existence of multiple maxima in the melting line. Previously, a possible link between the maximum in the melting line and liquid–liquid phase transition (LLPT) was suggested [2]. Also, changes in the short-range order of molten Na and Cs at high pressure have been correlated to the corresponding solid phase transitions [1–4]. Abrupt structural changes in other liquids such as Si, Ge, C [5] and N_2 [6] have been reported and the existence of LLPT was implicated. So far, the only case that has been confirmed unequivocally by experiments and theoretical calculations is liquid phosphorus [7], where the phase transition is due to change from a molecular to a polymeric structure at high pressure. In the case of monatomic liquid, analysis of the structures has not been as complete.

The high pressure structures of crystalline Li up to 60 GPa have been well characterized. At ambient pressure, Li adopts a 14 (8 + 6) coordinated bcc structure, which transfers to a compact 12-coordinated fcc structure at 7.5 GPa [8–10]. A structural transition from the fcc to a *cI*16 (with 16-atoms in a distorted bcc lattice) structure via an intermediate rhombohedral *hR*1 phase was found at 39 GPa [11]. Although the ambient melting temperature of Li is very low (453 K), its melting curve has only been determined over a very limited pressure range up to 8 GPa [12, 13] mainly due to the experimental difficulties in handling the light and reactive Li under high pressure. Recently, liquid Li under extreme pressure and temperature conditions up to 1 TPa and 3000 K have been studied with *ab initio* molecular dynamics [14]. The primary goal of the previous work [14] was to determine the melting temperature over a broad pressure range and at very high temperature. It was reported that a transition from a bcc-like to fcc-like local order occurred at 23 GPa in analogy to liquid Na [4]. However, there were not sufficient data and detailed analysis, particularly at the low pressure region, to support this suggestion. This conclusion was mainly based on the comparison of coordination numbers of the liquid structures with high pressure solid phases determined. It is important to recognize, due to experimental difficulties, that the high pressure crystal structures of Li were determined only at low temperature far from the melting point. It is noteworthy that it was shown recently that the high pressure structures of the related alkali metal Na near the melting point are very different from those determined at lower temperature [15]. In fact, the observed crystal structures close to melting at high pressure are quite complicated and

[3] Author to whom any correspondence should be addressed.

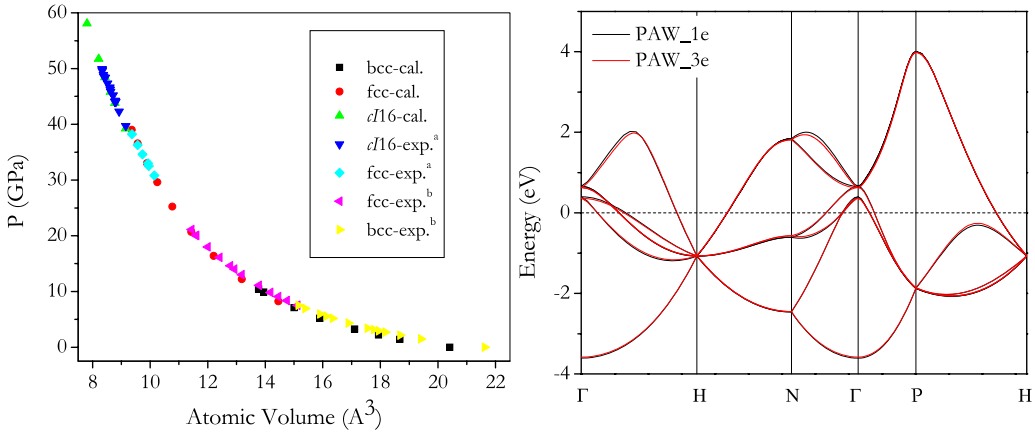

Figure 1. (Left) Comparison of calculated and experimental EOS ((a), [9] and (b), [13]) and (right) bandstructures for *cI*16 Li optimized at 58 GPa using the PAW potential, treating $2s^1$ (1e) and $1s^2 2s^1$ (3e) as valence states.

have different local environments as compared to the room temperature structures. Intuition would suggest that if a liquid indeed inherited the structure of the solid phase, the similarity in the short-range structural features should be most prominent close to the melting point. Moreover, the calculation of coordination number of a liquid is dependent on the choice of radial cutoff distance and subject to arbitrariness. Therefore, the examination of time-averaged properties, such as radial distribution functions and nearest neighbour coordinations, alone would not be sufficient to unambiguously define the local structure of a liquid.

In this paper, the structure of liquid Li under isothermal compression up to 60 GPa is revisited with first-principles molecular dynamics (MD) calculations. A more refined thermodynamic phase space (P, T) closer to the melting line than in previous work [14] is explored. The objectives of this study are (i) to examine the possible presence of LLPT and (ii) to expand on the previous studies to characterize the possible structural relationship between liquid and solid phases in a pressure region of 0–60 GPa where the high pressure crystal structures measured at low temperature are known [8–11]. Although other polymorphs in the vicinity of the melting line have not been established for Li, it is not unreasonable to speculate that they may be based on the similar observation for Na [15]. Therefore, the liquid structure may be more complex than the low temperature structures at similar pressure. In this work, apart from the examination of static structural factors, extensive analyses of the local order were performed through calculations of relevant orientation and order parameters and, in particular, study of the temperature-independent inherent structure [16] that is most appropriate for the characterization of local order in liquids. As will be shown below, detailed analyses of structural and electronic properties reveal several possible structural changes under compression. However, it was also found that the instantaneous liquid structure may not resemble the underlying low temperature crystal structure.

2. Computational details

First-principles MD calculations were performed on a model of liquid Li consisting of 128 atoms in a cubic box with periodic boundary conditions imposed. The generalized gradient approximation (GGA) [17] was used with a projector augmented wave (PAW) potential [18] replacing the 1s core electrons, as implemented in the Vienna *ab initio* simulation package (VASP) [19, 20]. We have verified the validity of the PAW (one electron) potential within the pressure range studied here by comparing the electronic and crystal structures of crystal Li obtained with the three-electron PAW potential. As shown in figure 1, the calculated equation of states (EOS) for the bcc, fcc and *cI*16 phases of Li using the 2s valence only PAW potential are in good agreement with experiments [9, 13]. Furthermore, no difference was found in the crystal structure and electronic bandstructure for *cI*16 Li at 58 GPa (figure 1) calculated with the two potentials. Electron orbitals were represented by plane waves with an energy cutoff of 140 eV in a $2 \times 2 \times 2$ Monkhorst–Pack k-point grid [21]. Simulations were performed at 600, 800 and 1000 K, respectively. At each temperature, MD calculations were performed within the pressure range between 0 and 60 GPa. These thermodynamic state points are chosen close to the melting line. The system was first equilibrated for 2.4 ps with a time step of 0.8 fs then followed by at least a 9.6 ps production run (some are as long as 24 ps) with the temperature controlled by a Nose–Hoover thermostat [22]. Thermodynamic equilibrium quantities (e.g. total energy and diffusion coefficient) converged very well within the MD simulation time window employed in the simulations. Diffusion coefficients were computed from the atomic mean square displacements. Electronic density of states (DOS) were obtained from the average of at least five random configurations extracted from the relevant MD trajectories using a dense k-point grid of $8 \times 8 \times 8$. Convergence was tested on selected configurations of liquid Li at 600 K and 20 GPa with a much denser k-grid of $12 \times 12 \times 12$, and no significant difference in the total DOS was found. Since liquid Li was predicted to be a solid [14] at 600 K between 10 and 35 GPa, it is necessary to verify the liquid state from the diffusion coefficient. In the ensuing presentation, results pertinent to a liquid are reported. In particular, properties of liquid Li along the 800 K isotherms are discussed in detail.

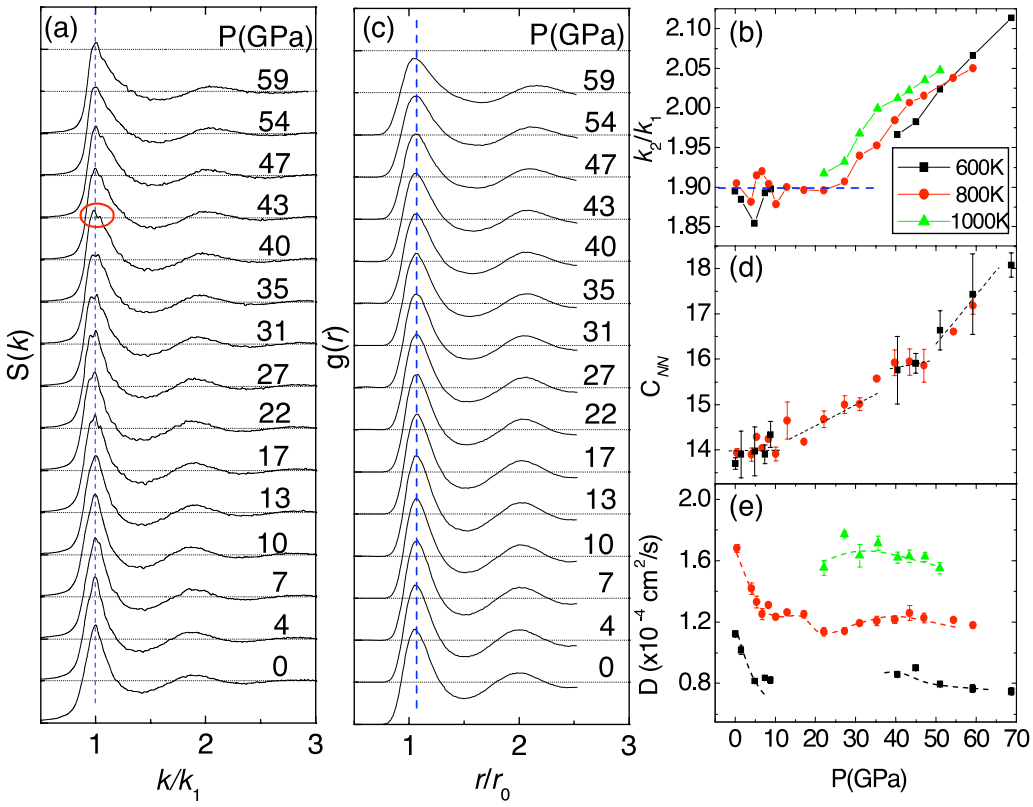

Figure 2. Pressure dependence of selected properties of liquid Li. (a) Static structure factor $S(k)$ and (c) radial distribution function $g(r)$ at 800 K. To facilitate the comparison between different densities [4], the wavevector k is scaled with the value at the first peak (k_1) and r is scaled by r_0. Dotted lines indicate the evolution of the second peak position with pressure. (b) k_2/k_1 ratio of $S(k)$, (d) coordination number C_{NN}, and (e) self-diffusion coefficients D as a function of pressure at 600, 800 and 1000 K. Dashed/dotted lines are guides to the eye. The circle in (a) indicates the splitting of the first peak in $S(k)$.

3. Liquid structure

The static structure factors $S(k)$ calculated from density autocorrelation functions for liquid Li at 800 K are plotted against k/k_1 (figure 2(a)) as well as the ratio k_2/k_1 at various pressures (figure 2(b)). k_1 and k_2 are defined as the respective position of the first and second band in $S(k)$. It is found that the shape of $S(k)$ does not change markedly at low pressures and is almost independent of the temperature. At 17 GPa the first band (k_1) starts to broaden and split into a doublet. The intensity of the shoulder at lower k increases with pressure and surpasses the main feature at 40 GPa (see red circle in figure 2(a)). The two features eventually merged at pressure over 47 GPa. Below 31 GPa the ratio k_2/k_1 (figure 2(b)) is nearly constant at ∼1.90, which is close to the value of 1.86 expected for a simple liquid metal [23] where the local potential interaction is isotropic (i.e. non-directional) [24]. Then it increases rapidly with pressure and reaches ∼2.05 at 60 GPa, the highest pressure considered in this study. A change in k_2/k_1 is indicative of a possible structural transition [23]. A larger k_2/k_1 ratio indicates that at pressures above 31 GPa liquid Li is no longer a simple isotropic liquid and the local structural environment is becoming more anisotropic. A similar trend on the variation of k_2/k_1 with pressure is also observed along the 600 and 1000 K isotherms but with the 'transition' shifts to a lower pressure at higher temperature, as shown in figure 2(b).

Figure 2(c) shows the evolution of the radial distribution function (RDF) $g(r)$ with compression at 800 K. To facilitate comparison at different densities, r is scaled by r_0, where $r_0 = \sqrt[3]{V/N}$, V is the volume of the simulation cell and N is the number of Li atoms inside this volume. The shape of the RDF does not change up to 10 GPa, indicating uniform compression at low pressure. At higher pressure the first peak broadens and the height decreases slightly. This trend becomes more evident at pressures higher than 40 GPa and, particularly, above 47 GPa. The average coordination numbers C_{NN}, obtained from integrating $g(r)$ to the first minimum, for liquid Li along the examined isotherms as a function of pressure are shown in figure 2(d). It can be seen that the effect of temperature on C_{NN} is minor. Below 10 GPa, C_{NN} is nearly constant at 14, which is similar to that of a bcc crystal. Upon further compression, C_{NN} increases, except in the small pressure interval between 40 and 47 GPa where the C_{NN} does not change noticeably. Consistent with the analysis on $S(k)$, the pressure dependence of C_{NN} also suggests possible structural changes around 10, 40 and 47 GPa. Incidentally, the calculated diffusion coefficients D (figure 2(e)) also show discontinuities at these pressures. The pressures at which these liquid–liquid structural changes occur are close to the bcc → fcc (7.5 GPa) and fcc → $cI16$ (42 GPa) transformations [11].

In earlier studies on liquid Li, Na and Cs [4, 14, 25], it was suggested that the liquid exhibits local order similar to that of the solids. In this study the RDF and C_{NN} of

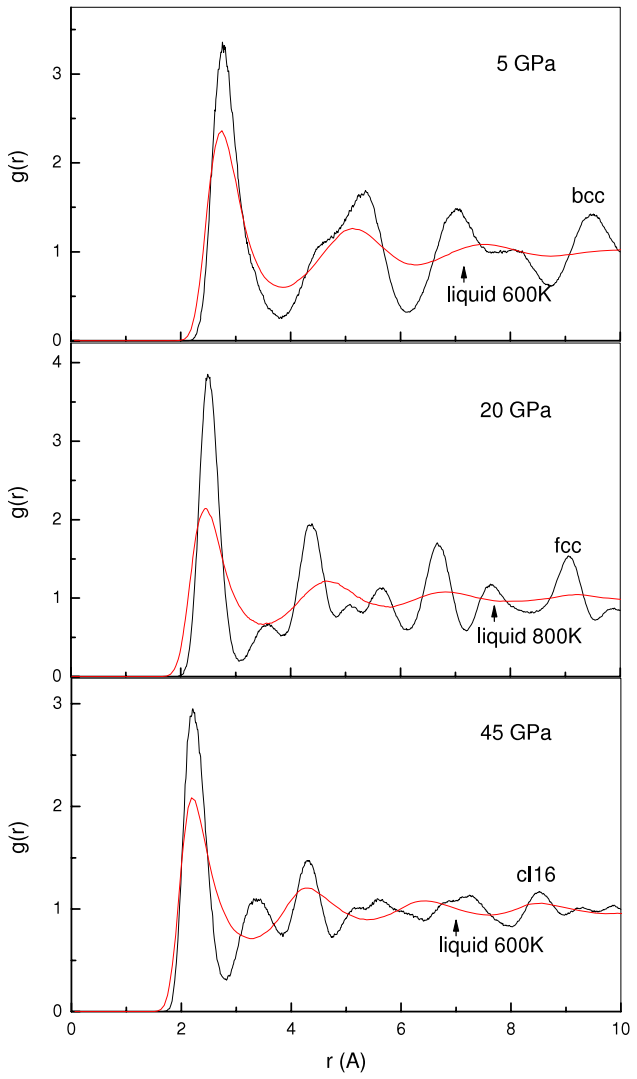

Figure 3. Comparison of RDF between liquid Li at (5 GPa, 600 K), (22 GPa, 800 K) and (45 GPa, 600 K) and the corresponding solid phases, i.e. bcc at 400 K, fcc at 400 K and *cI*16 at 300 K, respectively.

liquid Li at 5 GPa and 600 K were found to resemble a bcc solid (see figure 3). However, at 20 and 45 GPa, although positions of the first peak in the RDF are close to the corresponding fcc and *cI*16 solids, the C_{NN} are significantly different. To extract information on the local structure beyond the immediate neighbours, the bond angle distribution $g^{(3)}(\theta)$, a simple three-body correlation function, was calculated. Only the first two nearest neighbours that determine the local atomic arrangement [26] were considered. For illustration, results of liquid Li at 800 K are plotted in figure 4(a) at four selected pressures. At 0 GPa $g^{(3)}(\theta)$ has a peak at 70° and a broad hump around 110°. This distribution is similar to a bcc solid (70° and 109°). Under compression, a redistribution of 'bonds' is reflected in the shift of the principal peak to a higher angle which finally merges with the broad hump spanning over 80°–110° (see the distribution at 13 GPa). This peak becomes narrower upon compression. Above 35 GPa the bond angle distribution profile is similar to the *cI*16 phase which shows a narrower single peak centred at ∼105°.

To better define the local structure, a more precise geometrical order parameter is needed. The parameter W_6 is recognized as a good indicator for the characterization of global (spatial) orientational order in liquids [27]. For each atom, W_6 was calculated and averaged over 10 000 configurations using the same cutoff distance as for the RDF. The distribution of W_6 for liquid Li at 800 K is displayed in figure 4(b) at three typical pressures. Calculated W_6 distributions for fcc and bcc solids at 400 K are also shown for comparison. In the solids, the W_6 distributions are very narrow and centred at 0.013 for bcc and −0.013 for fcc structure. In comparison, W_6 distributions in liquid are very broad and nearly symmetric around 0.0 and are not sensitive to the pressure. A similar observation has been made in a previous study on liquid Na [28]. A more informative way to describe a liquid structure is to perform W_6 analysis on the inherent structures [16] obtained from quenching of instantaneous structures of the liquid. The inherent structure is a configurational mapping of arbitrary sets of atomic positions to relative minima on the potential energy hypersurface of the many body system. This approach isolates the 'static' effect by removing the vibrational distortion and diffusive contribution. This method has been proven to be invaluable in identifying hidden structure in liquids and has been applied broadly to the characterization of melting transitions. In our case, at each selected pressure and temperature, five independent configurations were chosen randomly from the MD trajectories. As shown in figure 4(c), at 4 GPa and 800 K a well-defined value of 0.014 for W_6, which is almost the same as in a bcc crystal (0.013), is found in two of the five inherent structures. While the sampling obviously is not exhaustive, at 600 K, the bcc-like W_6 was found in one of the five inherent structures. Further analysis revealed that the bcc-like inherent structure at 600 K exists only for 0.12 ps, roughly corresponding to two vibrational periods. The transient lifetime is even shorter for the two bcc-like inherent structures at 800 K which survived less than 0.096 ps. The transient lifetimes reported here are comparable to the survival time described in [14]. It was shown previously [14] at a similar pressure (3 GPa, $r_s = 3.06$), that the survival time (the temporal average of the transient lifetime) at a higher temperature of 1000 K is 0.04 ps. In this study, at 1000 K, no bcc-like inherent structure was found. These observations are not surprising since the local environment of a liquid is expected to change continuously with time. Thus, even though the temporal average radial and angular distributions show characteristic trends reminiscent of a bcc crystal, these pieces of evidence are not conclusive. The occasional solid-like local structures do exist in the liquid but they are transient structures and do not survive for a long time. At 22 GPa, W_6 of the inherent structures shows a narrow distribution around 0.0 that might indicate the enhancement of a local order, but these values are not close to that of either bcc or fcc structure. At 59 GPa, the distribution of W_6 is very broad and shows no preference to any ordered structure. As demonstrated here, although examinations of the RDF reveal that the liquid structures are broadly similar to the underlying high pressure solid phases, it is important to investigate the

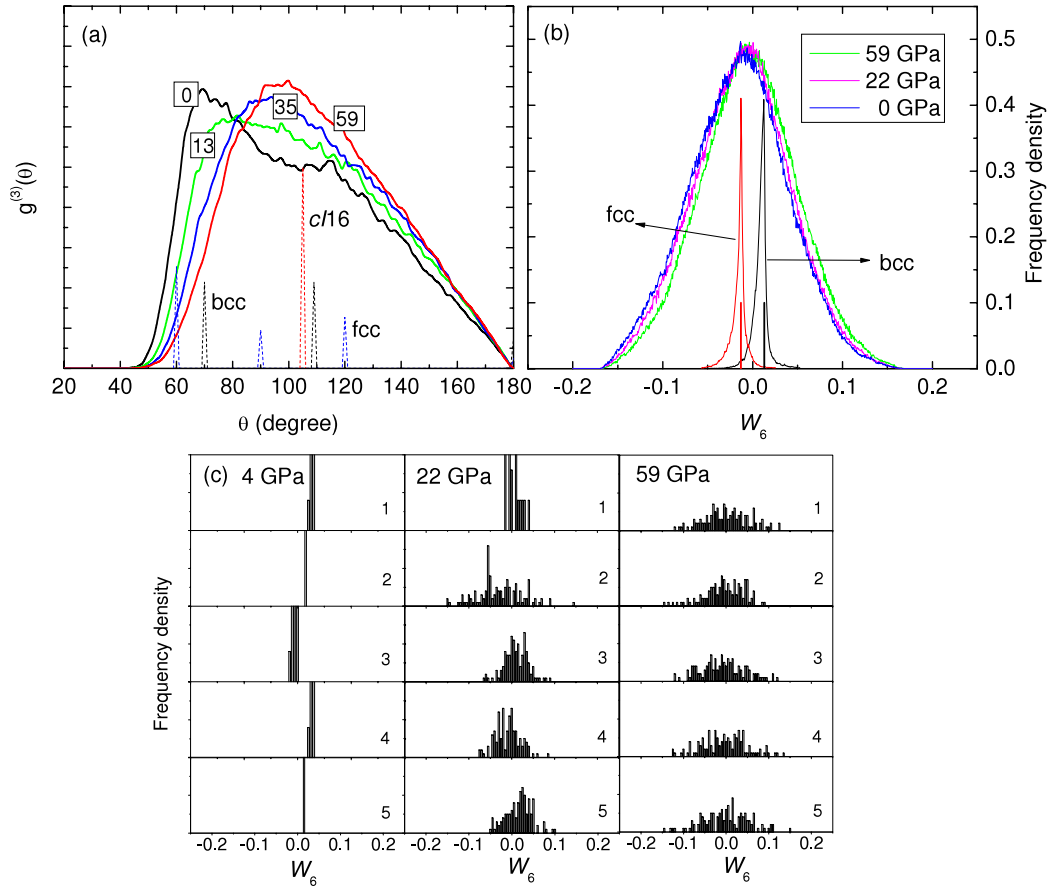

Figure 4. Structural analysis on liquid Li at 800 K. (a) Bond angle distribution function $g^{(3)}(\theta)$ presented at typical pressures of 0, 13, 35 and 59 GPa. The corresponding values for bcc, fcc and *cI*16 crystals are shown for comparison. (b) W_6 distribution at 0, 22 and 59 GPa. The bcc and fcc at 400 K are also shown for comparison. (c) Histogram of W_6 distribution for five calculated inherent structures at 4 (left panel), 22 (middle panel) and 59 GPa (right panel).

temporal variation of the order parameter(s) of the inherent structures.

4. Electronic structure

To probe the electronic origin of the structural changes, effects of compression and temperature on the angular momentum projected electronic DOS (PDOS) of liquid Li are analysed. At each pressure, to avoid overlap of atomic spheres and to minimize the interstitial space, the Wigner–Seitz radius was chosen to be half of the closest distance between two Li atoms. Near the Fermi level (E_F) the DOS is found to be composed mostly of Li p- with very small s-contribution (figure 5(a)). The DOS profiles show a strong resemblance to the corresponding high pressure solids [11] that the DOS at E_F was found to decrease with pressure. Upon compression, both s- and p-electron densities at E_F decrease while the s-character diminishes more rapidly. The increased occupation of the p-states with pressure is shown in the p–s ratio at E_F in figure 5(b). Below 10 GPa, the s→p electron transfer is very pronounced, indicating that the structural change, as in the corresponding solid phases, may be driven by the change in electronic structure. This is supported by the observation that the occupation of p-states increases slightly with increasing temperature which correlates very well with the predicted shift of the 'transition' (*vide supra*) to a lower pressure at high temperature. Finally, the valence bandwidth of liquid Li is found to increase with pressure, reaching a maximum around 30 GPa, and then decreases gradually with further compression (figure 5(c)). This trend is the same as that found in the solid [11] and has been explained elsewhere. In essence, this is the consequence of s → p hybridization leading to a fundamental change in the mode of chemical bonding from σ type to π type [29]. Significantly, the *cI*16 phase also shows a decrease in the valence bandwidth under compression, as shown in the liquid above 35 GPa.

The electron localization function (ELF) [30] is a powerful indicator to characterize the change in the electronic distribution as well as the chemical bonding. The ELF often resembles the charge density distribution but it has the added advantage in providing information on the tendency of the pairing of the electrons. Calculations of ELF on four instantaneous structures, selected randomly at 800 K and at pressures of 0, 10, 27 and 59 GPa, were performed and are compared in figure 6. Iso-surface plots with ELF = 0.85 show some valence electrons are already localized in cages formed by Li atoms even at 0 GPa. This observation is not too surprising since even for bcc Li under ambient pressure, the valence electrons have already been found to migrate

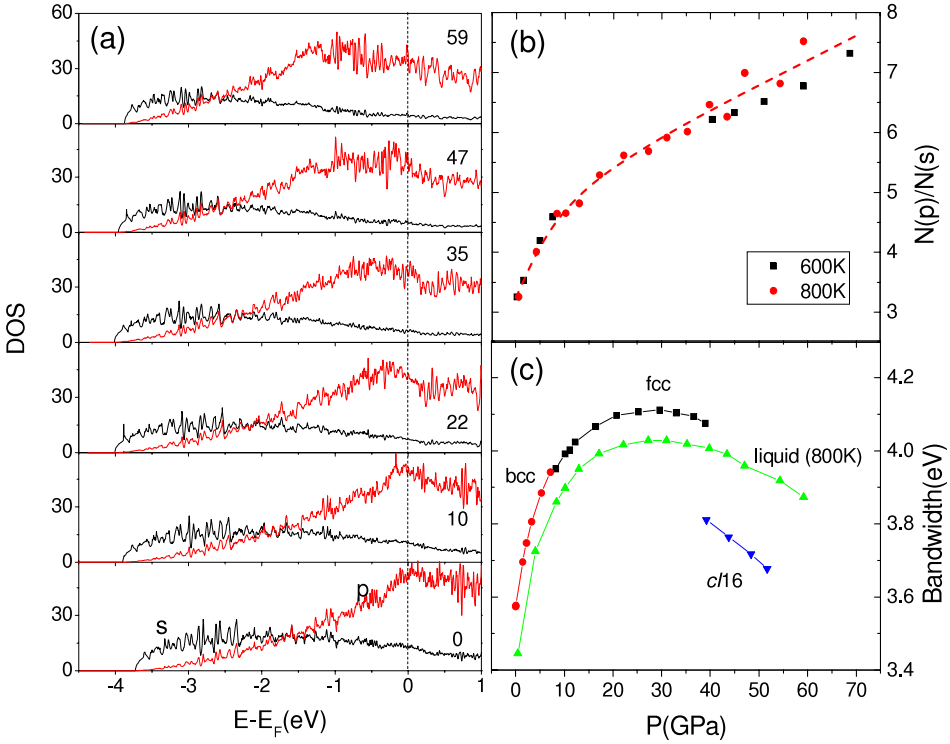

Figure 5. Electronic density of states of liquid Li at different pressures (GPa). (a) s- and p-contributions to the PDOS for liquid Li at 800 K. (b) Ratio of p-to-s PDOS at the Fermi level at 600 and 800 K. (c) Valence bandwidth for liquid at 800 K compared with the corresponding solids.

into interstitial sites [29, 31] due to better interaction via the overlap of the Li 2p orbitals. At higher pressure, overlaps between diffuse Li 2p orbitals become progressively stronger, leading to more significant electron localization in interstitial sites [31]. At 59 GPa, the maximum ELF value was found to be 0.94, indicating a very strong tendency of electron pairing in the interstitial regions. This observation is consistent with the earlier prediction on the concentration of electron density in the interstitial region, although previous calculations were performed at a much higher pressure of 150 GPa [14]. More significantly, it is shown here from the ELF that the electrons also prefer to be spin-paired. This phenomenon is akin to the high pressure (density) analogy of a Wigner crystal. It should be noted that the electron density has been found to localize in the interstitial region in the previous calculation on liquid Li at very high pressure and temperature [14].

5. Summary

Several structural and electronic transitions of liquid Li are found from *ab initio* molecular dynamics calculations near 10, 40 and 47 GPa over the temperature interval from 600 to 1000 K. The structural changes, which are akin to LLPT, are spread over a much wider pressure range due to atomic diffusion and do not exhibit the characteristics of first-order transitions as in the solids. The 'transition' pressure decreases slightly with temperature. Below 10 GPa, the liquid is compressed uniformly. At high pressure, the local structure becomes more anisotropic, indicating that the electronic interactions become more directional. The 'transition' pressures in the liquid are close to solid–solid phase transitions. Examinations of the RDFs and bond angle distributions agree with the previous study [14] showing that the temporal average liquid structures are indeed close to the underlying solids. However, analysis of bond orientation parameter W_6 and inherent structures provides additional and more detailed information on the local order. In a liquid, due to diffusion, the local structures are transient and change continuously. Thus, even though the RDFs may resemble that of the underlying high pressure phase, the instantaneous local order can be very different. The results highlight the ambiguity and arbitrariness in uniquely describing liquid structures. A RDF is the 1D projection of the spatial average of relative atomic positions and the angular (i.e. orientation) information is lost. In liquid Li, the W_6 orientation parameters cover a broad range spanning both the fcc and bcc structures. Only on rare occasions does the relative orientation between nearest neighbour atoms favour the crystalline environment. Finally, there is also the possibility that the low temperature crystal structure of a high pressure solid need not be the same as that near the melting point. The structural diversity near the solid–liquid phase boundary, particularly close to the behaviour change of the melting curve, as reported recently in Na [15], may be a general phenomenon. The variation of high pressure ice structures shows a similar behaviour bordering the liquid–solid phase boundary. For example ice III, V and VI possess very complex structures and display a variety of hydrogen-bond networks that may or may not be present in the liquid state [32].

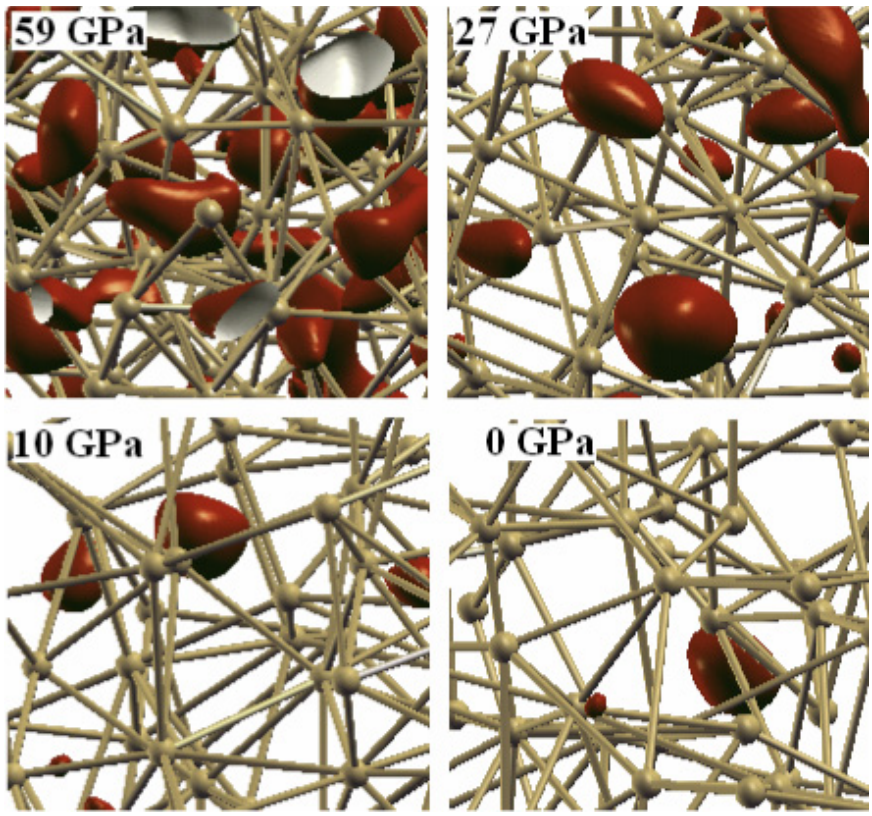

Figure 6. Electron localization function (ELF) at an iso-contour value of 0.85 for liquid Li at 800 K. The black and grey colour represent the outside and inside of the iso-surface, respectively. Li atoms are connected here if the separation is less than the first nearest neighbour peak in the RDF. Plots of the electron density show similar concentrations of electrons in the interstitial sites.

Acknowledgments

The authors wish to thank RIKEN RSCC for the generous allocation of computational resources. JST is a senior collaborative researcher at RIKEN.

References

[1] Gregoryanz E, Degtyareva O, Somayazulu M, Hemley R H and Mao H 2005 *Phys. Rev. Lett.* **94** 185502
[2] Falconi S, Lundegaard L F, Hejny C and McMahon M L 2005 *Phys. Rev. Lett.* **94** 125507
[3] Hernandez E R and Iniguez J 2007 *Phys. Rev. Lett.* **98** 055501
[4] Raty J-Y, Schwegler E and Bonev S A 2007 *Nature* **449** 448–52
[5] Jakse N and Pasturel A 2007 *Phys. Rev. Lett.* **99** 205702 and references therein
[6] Mukherjee G D and Boehler R 2007 *Phys. Rev. Lett.* **99** 225701
[7] Katayama Y, Mizutani T, Utsumi W, Shimomura O, Yamakata M and Funakoshi K 2000 *Nature* **403** 170–3
[8] Olinger B and Shaner W 1983 *Science* **219** 1071–4
[9] Hanfland M, Loa I, Syassen K, Schwarz U and Takemura K 1999 *Solid State Commun.* **112** 123–7
[10] Struzhkin V V, Hemley R J and Mao H K 1999 *Bull. Am. Phys. Soc.* **44** 1489
[11] Hanfland M, Syassen K, Christensen N E and Novikow D L 2000 *Nature* **408** 174–8
[12] Luedemann H D and Kennedy G C 1968 *J. Geophys. Res.* **73** 2795–805
[13] Boehler R 1983 *Phys. Rev.* B **27** 6754–62
[14] Tamblyn I, Raty J-Y and Bonev S A 2008 *Phys. Rev. Lett.* **101** 075703
[15] Gregoryanz E, Lundegaard L F, McMahon M I, Guillaume C, Nelmes R J and Mezouar M 2008 *Science* **320** 1054–8
[16] Stillinger F H and Weber T A 1983 *Phys. Rev.* A **28** 2408–16
[17] Wang Y and Perdew J P 1991 *Phys. Rev.* B **44** 13298–307
[18] Blöchl P E 1994 *Phys. Rev.* B **50** 17953–79
Kresse G and Joubert J 1999 *Phys. Rev.* B **59** 1758–75
[19] Kresse G and Hafner J 1993 *Phys. Rev.* B **47** 558–61
[20] Kresse G and Furthmüller J 1996 *Phys. Rev.* B **54** 11169–86
[21] Monkhorst H J and Pack J D 1976 *Phys. Rev.* B **13** 5188–92
[22] Nosé S 1984 *J. Chem. Phys.* **81** 511–9
Hoover W G 1985 *Phys. Rev.* A **31** 1695–7
[23] Waseda Y 1980 *The Structure of Non-Crystalline Materials* (New York: McGraw-Hill)
[24] Hansen J P and McDonald I R 1976 *Theory of Simple Liquids* (London: Academic)
[25] Falconi S and Ackland G J 2006 *Phys. Rev.* B **73** 184204
[26] González D J, González L E and Stott M J 2006 *Phys. Rev.* B **74** 014207
[27] Steinhardt P J, Nelson D R and Ronchetti M 1983 *Phys. Rev.* B **28** 784–805
[28] Hernandez E R and Iniguez J 2007 *Phys. Rev. Lett.* **98** 055501
[29] Rousseau R, Uehara K, Klug D D and Tse J S 2005 *ChemPhysChem* **6** 1703–6
[30] Becke A D and Edgecombe K E 1990 *J. Chem. Phys.* **92** 5397–414
Silvi B and Savin A 1994 *Nature* **371** 683–6
[31] Rousseau R and Marx D 2000 *Chem.—Eur. J.* **6** 2982–93
[32] For example see www1.lsbu.ac.uk/water